DISCLAIMER

This report was prepared as an account of work sponsored by an agency of the United States Government. Neither the United States Government nor any agency thereof, nor any of their employees, makes any warranty, express or implied, or assumes any legal liability or responsibility for the accuracy, completeness, or usefulness of any information, apparatus, product, or process disclosed, or represents that its use would not infringe privately owned rights. Reference herein to any specific commercial product, process, or service by trade name, trademark, manufacturer, or otherwise does not necessarily constitute or imply its endorsement, recommendation, or favoring by the United States Government or any agency thereof. The views and opinions of authors expressed herein do not necessarily state or reflect those of the United States Government or any agency thereof. Reference herein to any social initiative (including but not limited to Diversity, Equity, and Inclusion (DEI); Community Benefits Plans (CBP); Justice 40; etc.) is made by the Author independent of any current requirement by the United States Government and does not constitute or imply endorsement, recommendation, or support by the United States Government or any agency thereof.

ORNL/TM-2025/4038

Evaluate Compatibility of Alloy 244 in NaCl–$MgCl_2$

R. Pillai
S. Cambier
T. Lowe
A. Willoughby

July 2025

M3MT-25OR0904033

OAK RIDGE National Laboratory

ORNL IS MANAGED BY UT-BATTELLE LLC FOR THE US DEPARTMENT OF ENERGY

ORNL/TM-2025/4038

Advanced Materials and Manufacturing Technologies Program

EVALUATE COMPATIBILITY OF ALLOY 244 IN NaCl–$MgCl_2$

R. Pillai
S. Cambier
T. Lowe
A. Willoughby

July 2025

DOE Milestone: M3MT-25OR0904033

Prepared by
OAK RIDGE NATIONAL LABORATORY
Oak Ridge, TN 37831
managed by
UT-BATTELLE LLC
for the
US DEPARTMENT OF ENERGY
under contract DE-AC05-00OR22725

CONTENTS

LIST OF FIGURES

LIST OF TABLES

ABBREVIATIONS

BSE	backscattered electron
EDS	energy dispersive x-ray spectroscopy
fcc	face-centered cubic
HN	Hastelloy N
ORNL	Oak Ridge National Laboratory
TP	TerraPower

ACKNOWLEDGMENTS

This research was sponsored by the US Department of Energy, Office of Nuclear Energy, Advanced Materials and Manufacturing Technologies program under contract DE-AC05-00OR22725 with UT-Battelle LLC. The electron microscopy work was supported by the U.S. Department of Energy, Office of Nuclear Energy, Fuel Cycle R&D Program and the Nuclear Science User Facilities. The authors would like to thank Joanna Mcfarlane and Marie Romedenne for their thoughtful review of this report before publication.

ABSTRACT

Alloy 244 is a potential material of interest for molten salt reactor (MSR) developers employing molten chloride as fuel and coolant salts because of its improved mechanical properties compared to the austenitic stainless steel 316H and the Ni-base alloy Hastelloy-N. However, data are limited on the corrosion behavior of alloy 244 in molten chloride salts. Experimental data on the corrosion behavior of 244 in chloride salts will provide valuable data to MSR developers while simultaneously aiding in improving mechanistic understanding of the role of salt chemistry, alloying constituents and microstructure of 244. This task evaluated the compatibility of alloy 244 in two different eutectic NaCl–$MgCl_2$ salt mixtures. Similar corrosion behavior in terms of depths of attack and compositional changes in the alloy subsurface was observed after exposure in both salts for 500 h at 750°C. However, severe corrosion attack was observed after 500 h at 850°C in one of the chloride salt mixture. This was most likely due to the combined effects of the differences in the two salt chemistries, distinct microstructure of 244 at 850°C compared to 750°C, and the temperature dependence of the chemical interactions (thermodynamic and kinetic) between the alloying constituents.

1. INTRODUCTION

Alloy 244 is a potential material of interest for molten salt reactor (MSR) developers employing molten chloride as fuel and coolant salts because of its improved mechanical properties compared with the austenitic stainless steel 316H and the Ni-base alloy Hastelloy-N (HN). However, data are limited on the corrosion behavior of alloy 244 in molten chloride salts. Keiser et al. (Keiser et al. 2022) performed corrosion testing of a range of candidate bearing materials in the ternary 20NaCl–40$MgCl_2$–40KCl (mol %) mixture for 500 h at 750°C. Alloy 244 showed comparable attack to that of alloy 230 but had a much higher attack than Inconel 600. This was a surprising result considering the Cr content of alloy 244 (8 wt %) is significantly lower than the 16 wt % in Inconel 600. Experimental data on the corrosion behavior of 244 in chloride salts will provide valuable data to MSR developers while simultaneously aid in improving mechanistic understanding of the role of salt chemistry, alloying constituents and microstructure of 244. This task evaluated the compatibility of alloy 244 in two NaCl–$MgCl_2$ salt chemistries (NaCl–$MgCl_2$ purified using the well-established process at Oak Ridge National Laboratory [ORNL] (Mayes et al. 2018) and a salt batch provided by TerraPower [TP]) by performing static capsule tests in Mo capsules.

2. EXPERIMENTAL PROCEDURE

Specimens of alloy 244 were machined from a 5 cm thick alloy 244 plate provided in a solution annealed by Haynes International. The measured composition of the alloy is given in Table 1.

Table 1. Compositions of the studied alloys (wt %) determined by plasma/combustion analyses

Element	Ni	Cr	Fe	Mn	Mo	W	C
Amount (wt %)	61.9	8	1.1	0.3	22.4	6	0.045

Static capsule tests were conducted in Mo capsules using rectangular (~10 × 12 × 1.5 mm) alloy 244 specimens. The Mo capsules were loaded and welded shut with the salt and the specimens and were placed into a larger type-316 stainless steel capsule, which was also welded shut to provide secondary containment and prevent oxidation of the Mo capsule. All steps were conducted in an Ar-filled glove box (with controlled atmosphere and impurity levels less than 1 ppm O_2 and H_2O). The capsules were exposed in a box furnace at 750°C and 850°C for up to a maximum exposure time of 500 h. After cooling, the capsules were opened in the same glove box and were cleaned in 50°C H_2O for several hours to remove the salt deposits. The samples were weighed for mass change with a Mettler Toledo model XP205 balance with an accuracy of ±0.04 mg (< 0.01 mg/cm^2). Postexposure specimens were cross-sectioned for metallographic analyses.

Table 2. Test matrix for the creep tests

Alloy	Temperature (°C)	Time (h)	Salt
244: solution annealed	750, 850	100, 500	TP
	750, 850	500	ORNL

The NaCl–$MgCl_2$ eutectic salt used in this study was prepared with 58.5 mol % anhydrous NaCl salt and 41.5 mol % anhydrous $MgCl_2$ salt. The salt was homogenously mixed and purified following an established purification procedure for chloride salts (Mayes et al. 2018). The trace impurities of the

$NaCl–MgCl_2$ eutectic salt mixture were identified by inductively coupled plasma mass spectrometry analysis in which the most prominent impurity elements and the corresponding concentrations were 1.5 ppm Cr, 10.8 ppm Fe and 1.4 ppm Ni (all by weight). A second batch of the eutectic $NaCl–MgCl_2$ was provided by TP, which will be designated as TP salt hereafter. The measurement of the oxygen impurities in both batches of salts is currently ongoing. The experimental program is summarized in Table 2.

Postexposure specimens were cross-sectioned for metallographic analyses. The mounted samples were ground to 1,200 grit with SiC grinding papers and subsequently polished with diamond pastes to 1 μm surface finish. The final preparation step involved preparation with colloidal silica. Microstructural characterization to measure compositional changes and identify phase transformations was performed using scanning electron microscopy, backscattered electron (BSE) microscopy (ZEISS), and energy dispersive x-ray spectroscopy (EDS; Octane Elect EDS/EDX with Super Silicon Drift Detector).

3. RESULTS

The initial microstructure of alloy 244 in the solution annealed state consists of the γ-face-centered cubic (fcc) matrix with μ-phase (chemical formula $Cr_{20}Mo_{43}Ni_{37}$, hexagonal crystal system), P-phase (chemical formula $Cr_9Mo_{21}Ni_{20}$,orthorhombic crystal system), and M_6C type carbides (Fahrmann, Srivastava, and Pike 2012). The two-step precipitation aging heat treatment (16 h at 760°C → furnace cooling → 32 h at 649°C → air cool) results in Ni_2(Cr, Mo, W) domains (body-centered orthorhombic Pt_2Mo structure type) and the (Mo, W)-rich μ-phase with zones denuded in Mo and W near the grain boundaries (Fahrmann, Srivastava, and Pike 2012). Long-term aging (1,000 h) at 760°C transformed the alloy to the microstructure to be γ-fcc + μ-phase (Fahrmann, Srivastava, and Pike 2012). Although the stability of the Ni_2(Cr, Mo, W) domains has not been studied at temperatures greater than 760°C, based on the disappearance of the phase after long-term aging at 760°C, it can be assumed that the phase will most likely not be stable at the higher test temperature of 850°C. Figure 1 shows the BSE images of the alloy 244 microstructure after 100 h at 750°C (Figure 1a) and 850°C (Figure 1b). The microstructure after 100 h at 750°C shows the Ni_2(Cr, Mo, W) domains with (Mo, W)-rich phases and the denuded zones near the grain boundaries. However, after 100 h at 850°C, no Ni_2(Cr, Mo, W) domains were visible, and the microstructure was primarily γ-fcc matrix + (Mo, W)-rich phases at grain boundaries.

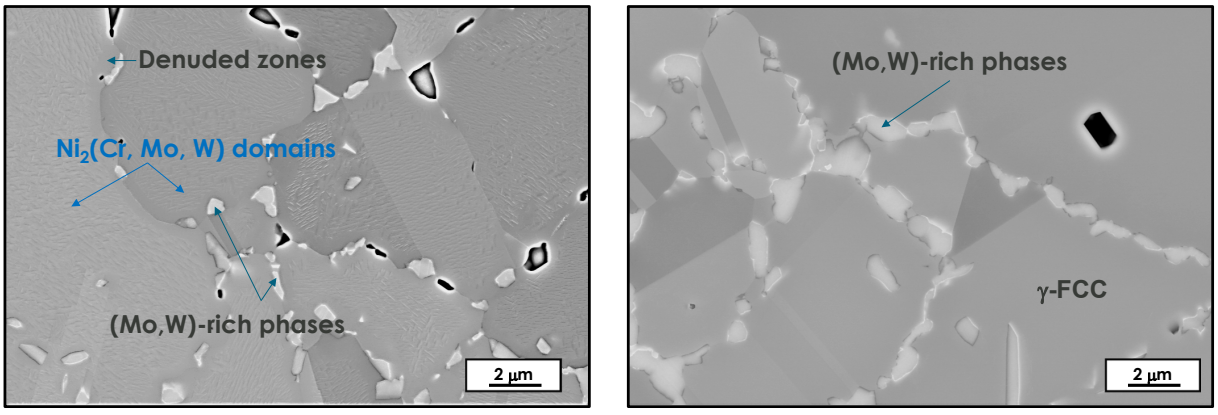

(a) (b)

Figure 1. BSE images of the solution annealed alloy 244 microstructure after 100 h at (a) 750°C and (b) 850°C.

The measured mass losses of the alloy 244 specimens after 500 h at 750°C and 850°C in the ORNL and TP eutectic $NaCl–MgCl_2$ salt mixtures are given in Figure 2a and Figure 2b, respectively. The mass loss

was comparable after 500 h at 750°C between the two salts, but a significantly higher mass loss was observed for the exposure in the ORNL salt at 850°C.

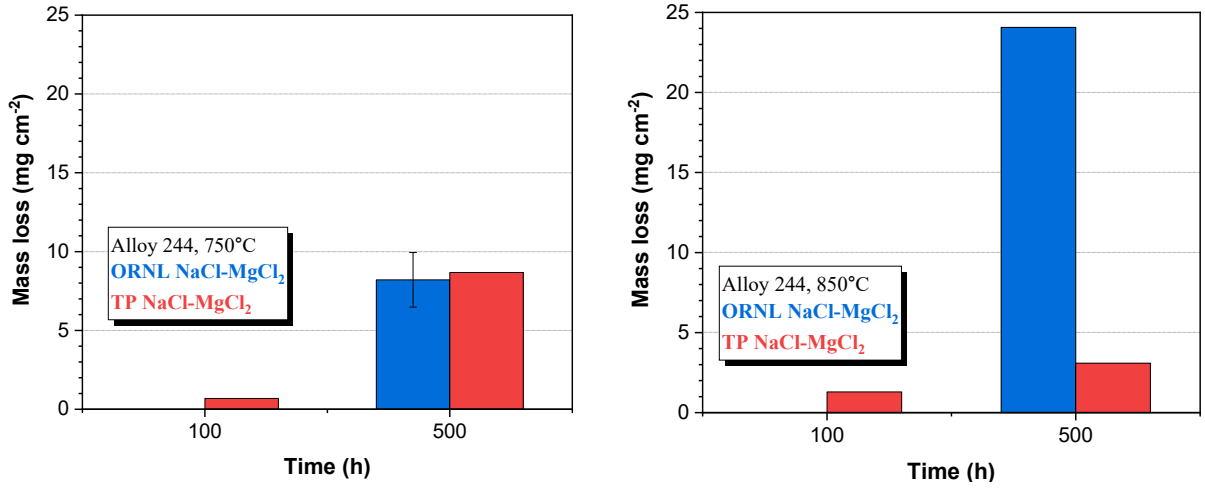

(a) (b)

Figure 2. Measured mass loss in alloy 244 specimens after 500 h at (a) 750°C and (b) 850°C in the (blue) ORNL and (red) TP eutectic NaCl–$MgCl_2$ salt mixtures.

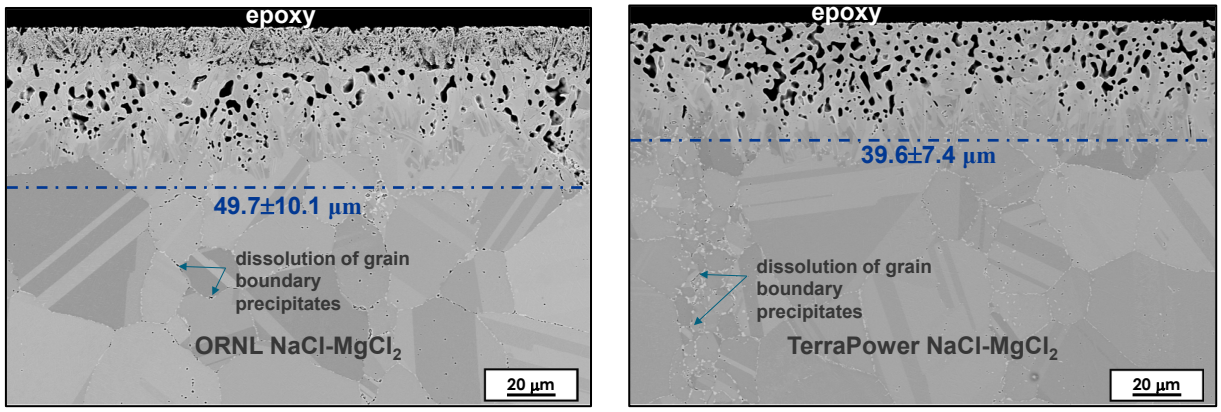

(a) (b)

Figure 3. BSE images of the cross sections of alloy 244 specimens after 500 h at 750°C in (a) ORNL and (b) TP eutectic NaCl–$MgCl_2$ mixtures.

Figure 3 shows the BSE images of the cross sections of alloy 244 specimens after 500 h at 750°C in the ORNL (Figure 1a) and TP (Figure 1b) eutectic NaCl–$MgCl_2$ mixtures. Similar depths of attack were measured for the exposures in the ORNL salt (49.7 ± 10.1 µm) and in the TP salt (39.6 ± 7.4 µm). The depth of attack for these measurements was the visual evidence for alloy dissolution (e.g., pore formation). The corrosion morphology at the alloy's surface is different between the two salts, with an acicular (needle shaped) microstructure closer to the alloy's surface. Such a microstructure is not visible in the case of the exposure in the TP salt. Beyond the visually evident corrosion affected zone, dissolution of grain boundary precipitates was observed, suggesting that the corrosion induced compositional changes affect the phase stabilities beyond the corrosion affected zone.

Figure 4 shows the BSE images of the cross sections of alloy 244 specimens after 500 h at 850°C in the (a) ORNL and (b) TP eutectic NaCl–$MgCl_2$ mixtures. In this case, a significantly higher depth of attack was observed for exposures in the ORNL salt (72.5 ± 9.1 µm) compared with the TP salt (10.2 ± 3.5 µm). A more frontal corrosion attack and the presence of O-rich areas (not shown here) suggested higher impurity content in the ORNL salt. The acicular corrosion morphology observed in the case of the exposure in the ORNL salt at 750°C was not observed at 850°C. Whether the absence of Ni_2(Cr, Mo, W) domains are accelerating corrosion in the ORNL salt at 850°C is a subject of ongoing investigations. Furthermore, the considerable differences in attack observed at 850°C and the preliminary observations of O-rich areas require a detailed comparison of the two salt chemistries. Chemical analyses to quantify impurity contents of the two salts is ongoing. Similar to the exposures at 750°C, dissolution of the (Mo, W)-rich precipitates was observed both within the grains and at grain boundaries.

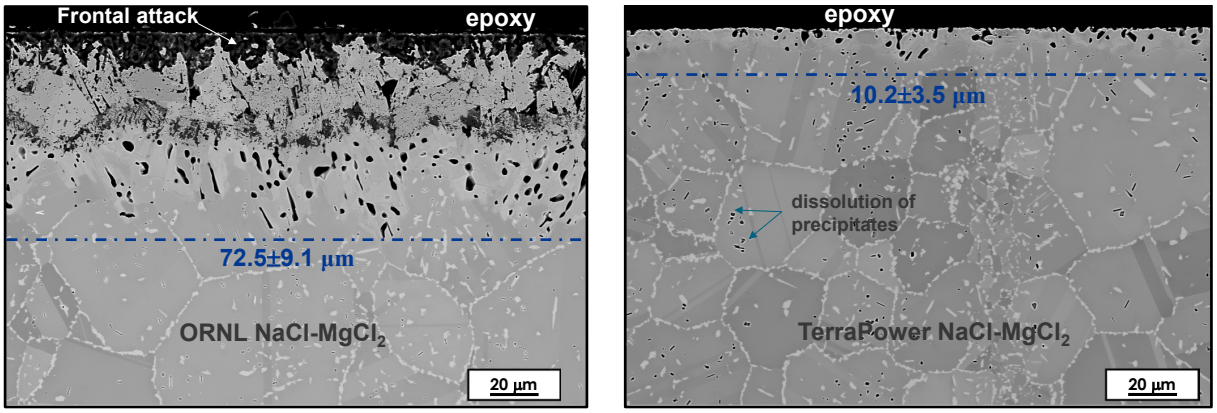

(a) (b)

Figure 4. BSE images of the cross sections of alloy 244 specimens after 500 h at 850°C in (a) ORNL and (b) TP eutectic NaCl–$MgCl_2$ mixtures.

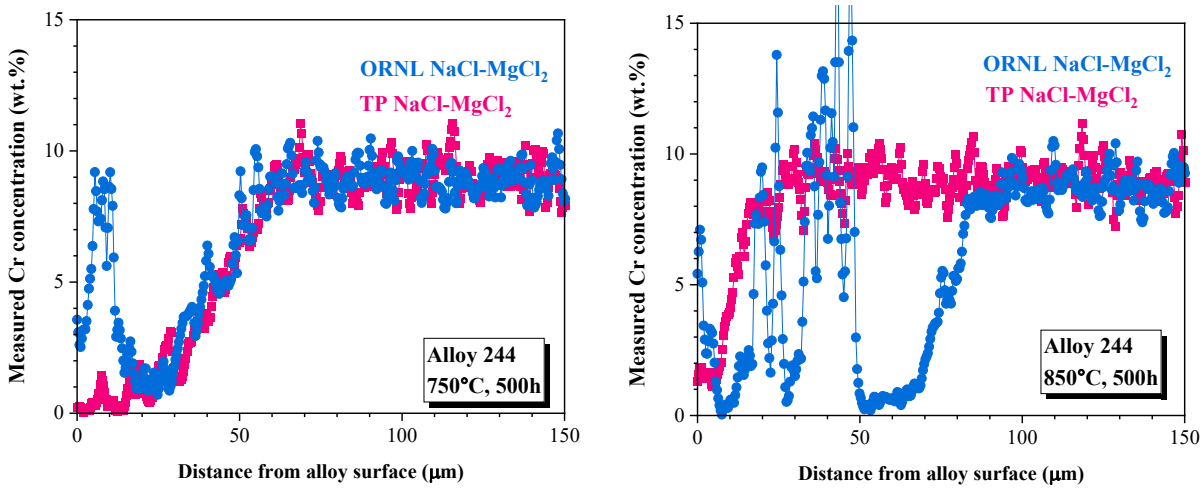

(a) (b)

Figure 5. Measured Cr concentration profiles (average of three EDS lines) in alloy 244 after exposure in the ORNL and TP eutectic NaCl–MgCl2 salt mixtures for 500 h at (a) 750°C and (b) 850°C.

Figure 5 shows the measured Cr concentration profiles (average of 3 EDS lines) in 244 after exposure in the ORNL and TP eutectic NaCl–$MgCl_2$ salt mixtures after 500h at 750°C (Figure 5a) and 850°C (Figure 5b). The concentration profiles show similar Cr depletion in both salts at 750°C which agrees with the observed mass change (Figure 2a) and depths of attack (Figure 3a). The significantly higher mass change and depth of attack observed in the ORNL salt at 850°C is confirmed with the measured deeper Cr depletion (Figure 5b).

Figure 6 shows the measured Mo concentration profiles (average of three EDS lines) in alloy 244 after exposure in the ORNL and TP eutectic NaCl–$MgCl_2$ salt mixtures for 500 h at 750°C (Figure 5a) and 850°C (Figure 5b). Similar Cr depletion profiles resulted in similar enrichment for Mo in the corrosion affected zone at 750°C. Interestingly, the much higher Mo enrichment caused by higher Cr depletion for the exposures in the ORNL salt did not necessarily result in suppression of corrosion, with the expectation that higher Mo contents would retard any subsequent corrosion.

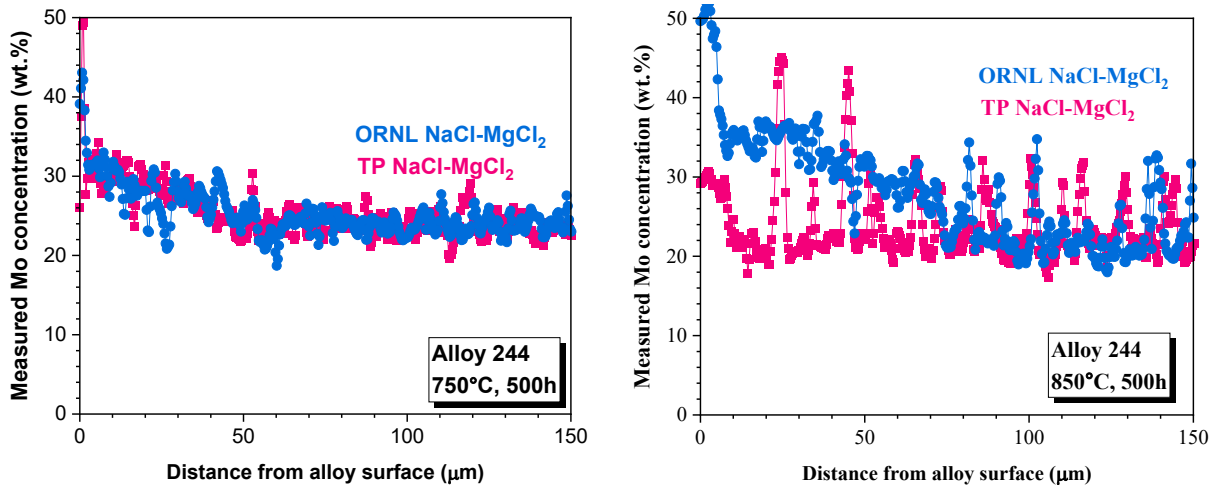

Figure 6. Measured Mo concentration profiles (average of three EDS lines) in alloy 244 after exposure in the ORNL and TP eutectic NaCl–$MgCl_2$ salt mixtures for 500 h at (a) 750°C and (b) 850°C.

4. DISCUSSION

Despite the low Cr content in 244, the alloy showed considerable attack in both chloride salts at 750°C. As shown previously by Pillai et al. ,(Pillai, Raiman, and Pint 2021a; Pillai et al. 2023), (Pillai, Raiman, and Pint 2021a; Pillai et al. 2023), corrosion in molten salts is governed by the chemical activity of Cr rather than its concentration and the diffusion kinetics of Cr in the alloy. Although 244 has a similar Cr content as HN, the Cr chemical activity is about twice the value in HN due to the presence of W (based on thermodynamic calculations). Pillai et al. (Pillai et al. 2023) have demonstrated the role of Cr and W interactions on the corrosion behavior of alloy 230 in molten chloride salts. The authors employed coupled thermodynamic-kinetic modeling to illustrate the role of W in increasing Cr activity in alloy 230 which results in a slower decrease in surface Cr activity compared to alloy 740H which does not contain W. The higher surface Cr activity results in accelerated corrosion in 230 which was validated with experimental results. Simultaneous enrichment of Mo in the alloy subsurface during corrosion induced depletion of Cr due to molten salt corrosion has been observed previously for Ni-base alloys HN (Koger 1972) and C-276 (Pillai, Raiman, and Pint 2021b). The reduced susceptibility of Mo to molten salts is expected to further suppress corrosion on the surface, although there is no conclusive experimental evidence for this in the literature. The role of the combined effect of these alloying constituents in the corrosion behavior of 244 needs further investigations.

The lower corrosion observed in the TP salt at 850°C compared to at 750°C might seem encouraging. However, it must be mentioned that these are results from static tests and flowing tests for 244 are essential to simulate reactor operating conditions and evaluate the influence of thermal gradients and mass transfer processes. Furthermore, there is increasing evidence for the weak temperature dependence of depletion of Cr in molten salts which suggests that the amount of Cr depleting in the salt does not continuously increase with temperature (Yingling et al. 2023). The differences in the two salt chemistries which can either be higher O impurities in the ORNL salt or potential redox additions in the TP salt most likely accelerate corrosion at 850°C in the ORNL salt and suppress corrosion in the TP salt at the higher temperature. Ongoing analyses of the ORNL and TP salt chemistries before and after corrosion tests will provide more insights. Ultimately, the role of the changes in phase stabilities in alloy 244 from 750°C to 850°C in governing corrosion requires a more detailed analyses.

5. CONCLUSIONS

Alloy 244 showed significant attack at 750°C in both salts but reduced attack in the TP salt at 850°C. Preliminary investigations suggest that a combined effect of the higher O impurities in the ORNL salt and the absence of the Ni_2(Cr, Mo, W) domains may cause increased corrosion in the ORNL salt at 850°C. A significantly higher enrichment of Mo in the alloy subsurface at 850°C due to increased Cr depletion did not suppress continued corrosion. Future work will focus on evaluating the combined effects of the differences in the two salt chemistries, distinct microstructure of 244 at 850°C compared to at 750°C and the temperature dependence of the chemical interactions (thermodynamic and kinetic) between the alloying constituents on the observed corrosion behavior of 244.

6. REFERENCES

Fahrmann, M., S. K. Srivastava, and L. M. Pike. 2012. "Development of a New 760°C (1400°F) Capable Low Thermal Expansion Alloy." *Superalloys 2012*: 769-777. <Go to ISI>://WOS:000324518300085.

Keiser, James R., Xin He, Dino Sulejmanovic, Jun Qu, Kevin R. Robb, and Keith Oldinski. 2022. "Material Selection and Corrosion Studies of Candidate Bearing Materials for Use in Molten Chloride Salt." *Journal of Solar Energy Engineering* 145 (2). https://doi.org/10.1115/1.4054507. https://doi.org/10.1115/1.4054507.

Koger, J. W. 1972. *Evaluation of Hastelloy N alloys after nine years exposure to both a molten fluoride salt and air at temperatures from 700 to 560$sup 0$C.* Oak Ridge National Lab., Tenn. (USA) (United States). https://www.osti.gov/biblio/4468052

https://www.osti.gov/servlets/purl/4468052.

Mayes, Richard T., James Matthew Kurley Iii, Phillip W. Halstenberg, Abbey McAlister, Dino Sulejmanovic, Stephen S. Raiman, Sheng Dai, and Bruce A. Pint. 2018-12-13 2018. *Purification of Chloride Salts for Concentrated Solar Applications.* ORNL/LTR-2018/1052, ORNL (United States: ORNL). https://www.osti.gov/biblio/1506795

https://www.osti.gov/servlets/purl/1506795.

Pillai, R., S. S. Raiman, and B. A. Pint. 2021a. "First steps toward predicting corrosion behavior of structural materials in molten salts." *Journal of Nuclear Materials* 546: 152755. https://doi.org/ARTN 152755

10.1016/j.jnucmat.2020.152755. <Go to ISI>://WOS:000614811200010.

---. 2021b. "First steps toward predicting corrosion behavior of structural materials in molten salts." 546: 152755. https://doi.org/10.1016/j.jnucmat.2020.152755. http://dx.doi.org/10.1016/j.jnucmat.2020.152755.

Pillai, R., D. Sulejmanovic, T. Lowe, S. Raiman, and B.A. Pint. 2023. "Establishing a design strategy for corrosion resistant structural materials in molten salt technologies." *JOM* 75: 994-1005.

Yingling, J. A., J. Schorne-Pinto, M. Aziziha, J. C. Ard, A. M. Mofrad, M. S. Christian, C. M. Dixon, and T. M. Besmann. 2023. "Thermodynamic measurements and assessments for LiCl-NaCl-KCl-UCl3 systems." *The Journal of Chemical Thermodynamics* 179: 106974. https://doi.org/https://doi.org/10.1016/j.jct.2022.106974. https://www.sciencedirect.com/science/article/pii/S0021961422002531.